電気学会論文誌●（●●●●●●●部門誌）
IEEJ Transactions on ●●●●●●●●●●●●●●●
Vol.●● No.● pp.●-● DOI: ●.●●/ieejeiss.●●.●

Paper

Reduction of Reflected Power Loss in an AC-DC Converter for Wireless Power Transfer Systems

Keisuke Kusaka*, Student Member, Jun-ichi Itoh*[a], Member

(Manuscript received Jan. 00, 20XX, revised May 00, 20XX)

This paper discusses a method to reduce reflected power in an AC-DC converter in high-frequency wireless power transfer systems. First, conventional capacitor input-type rectifiers with silicon carbide (SiC) and gallium nitride (GaN) diodes are experimentally tested. From an analysis of the results, it is confirmed that the reflected power occurs at the input stage of the rectifiers owing to impedance mismatching. The reflected power should be suppressed because it will decrease the transmission efficiency.

In order to solve the above-mentioned problem, an AC-DC converter that implements input impedance matching is proposed in the last half of the paper. This paper presents the basic characteristics of the AC-DC converter and the experimental results, which show that the input impedance of the AC-DC converter enables a conversion from 13.56 MHz AC to DC with an input impedance of 29.6 + j0.51 Ω. Thus, the reflected power is suppressed by 37.8% compared with the conventional capacitor input-type diode bridge rectifier with a load resistance of 25 Ω. From the experimental results, it is confirmed that the AC-DC converter is a valid circuit configuration for wireless power transfer systems.

Keywords : wireless power transfer, AC-DC converter, high-frequency, input impedance matching

1. Introduction

Wireless power transfer methods such as the electromagnetic induction method, the micro-wave power transfer and the laser transfer have been attracted in community[1-5]. However, these wireless power transfer methods have issues about the efficiency and transmission distance. In the electromagnetic induction method, the transmission distance of the wireless power transfer which can maintain the transmission efficiency at high is limited up to only a few centimeters due to the effect of leakage inductances. On the other hand, the micro-wave and the laser transfer methods can transfer power wirelessly in a long transmission distances, however these methods have insufficient of power conversion efficiency between an electric energy and a radioactive energy of electromagnetic waves[3-6].

Recently, the wireless power transfer using magnetic resonant coupling (MRC), which is reported by A. Karalis et al. in 2007, has been intensively in recent years[7-14]. The MRC shows better features compared with the conventional wireless power transfer methods such as the electromagnetic induction and the microwave power transfer methods. First, the MRC allows a wireless power transfer in a middle-range transmission distance such as a few dozen of centi-meters at high efficiency of over 90%[15]. Second, the declination of the transmission efficiency caused by a position gap of the transmitting coils is relatively small. These advantages are reason of the characteristic constructions from the transmission coils. The transmitting coils have high quality factor Q owing to the low parasitic resistance of the coils. The high quality factor allows an efficient wireless power transfer in a middle-range transmission distance even when the coupling coefficient k is small because the transmitting efficiency is proportional to the product of a quality factor and a coupling coefficient[16]. Note that a coupling coefficient decreases inversely with a cube of distance. Considering to apply the wireless power transfer with MRC in the battery chargers for electrical vehicles (EV), the coil for the transmitting side and also for receiving side are planted on the ground of parking areas, and underneath of EVs, respectively. This technology can improve the convenience for users because users are not required to charge the battery with electrical cables[17].

In the wireless power transfer system with the MRC, the size of the transmitting coils depends on the transmitting frequency[12]. The wireless power transfer systems are expected to operate in high-frequency in order to achieve high power density. Additionally, MRC should be operated in the industrial, scientific and medical (ISM) band because noise from the wireless power transfer system is prohibited to influence the operation of neither the electronic devices nor the radio communication equipment. For this reason, 13.56 MHz is used as the transmitting frequency in this paper.

For this reason, an AC-DC converter, which can convert from 13.56 MHz-AC to DC, is required in the receiving side of the wireless power transfer system. In addition, an impedance matching is necessary in such high-frequency region in order to suppress the occurrences of reflected power[18]. A reflected power occurs at boundary points of the impedance when impedances are different from the input impedance of an AC-DC converter with the characteristic impedance of the transmission line[19]. In order to suppress reflected power, an input impedance of an AC-DC converter should be matched to the characteristic impedance of the transmission line. However, the input impedance matching methods for the AC-DC converter has not been reported in such as the high input frequency operation on the AC-DC converter are not reported. It is difficult to make an input impedance matching

a) Correspondence to: Jun-ichi Itoh. E-mail: itoh@vos.nagaokaut.ac.jp
* Nagaoka University of Technology
1603-1, Kamitomioka-machi, Nagaoka, Niigata, Japan 940-2188

because the high input frequency constrains the latitude of the circuit configurations.

This paper proposes and validates the AC-DC converter which achieves the power conversion from 13.56-MHz AC to DC without high-frequency switching. Additionally, the unity power factor is achieved by simple circuit configuration using a LC resonance.

The first section in this paper describes the principle of the MRC and the experimental setup with MRC. Secondly, the conventional capacitor input type diode bridge rectifiers (CI-DBRs) with wide-band gap semiconductor devices are tested as an AC-DC converter in the receiving side. The analysis of the experimental results confirmed the effect of the input impedance matching. Then, the required conditions for input impedance matching of AC-DC converters are clarified. Thirdly, the AC-DC converter which can achieve the input impedance matching is proposed in order to suppress reflected power. The proposed circuit is validated based on the simulation and experimental results.

2. Wireless Power Transfer System

2.1 Peripheral Circuits Fig. 1 illustrates the configuration example of the wireless power transfer system with MRC. The system consists of a PWM rectifier, a high-frequency inverter, a transmission part, an AC-DC converter and a battery. Generally, the high-frequency inverter is placed on the output stage of the PWM rectifier for actual uses. However, PWM rectifiers do not affect the wireless power transfer system because a role of the PWM rectifier is conversion from commercial frequency AC to DC. Additionally, this paper aims to evaluate the effect of the reflected power which occurs at input stages of the AC-DC converters. Hence, the PWM rectifier and the high-frequency inverter are not discussed in this paper.

The AC-DC converter, which has the battery as a load is place on the EV. In this paper, the AC-DC converters in the receiving side are discussed. A reflected power occurs at the boundary points of impedances owing to impedance mismatching when circuits are operated in a high-frequency. For this reason, a transmitting coil is connected from an output stage of an inverter via a coaxial cable with the characteristic impedance of 50 Ω. Similarly, a coaxial cable is used between the receiving coil and the AC-DC converter.

In the wireless power transfer systems with MRC, the size of transmission coils depends on the transmission frequency. Thus, a high-frequency transmission is desired from the standpoint of a power density of the wireless power transfer system. In this paper, the transmission frequency of 13.56 MHz that meets the ISM band is used.

2.2 Configuration of Experimental System Fig. 2 shows the system configuration of the experimental setup of the wireless power transfer system with MRC. The system consists of a function generator (FG), a radio frequency (RF) power supply which has the output impedance of 50 Ω, two resonance coils and a load. Signal from the FG is amplified by RF amplifier. The RF amplifier which can control the output travelling power is composed by an A-class linear amplifier in the test bench. The RF amplifier can output an arbitrary travelling power up to 500 W. Note that the output impedance of the RF amplifier is 50 Ω. The outputted power is delivered to the load in the receiving side using a magnetic resonant where the P_{in} is the power which is supplied to the transmitting coil and the P_{out} is the power which is picked up from the receiving coil. Thereby transmitting efficiency is defined by

$$\eta_T = \frac{P_{out}}{P_{in}} \times 100\ [\%] \quad \cdots\cdots (1)$$

Table 1 shows the specifications of the open-end resonance coils, which is used for the experiments, where the R_{ohm} is a calculation value of an ohmic loss with considering skin effect. Also, the inductance L and the capacitance C are measured by a LCR meter (HIOKI, 3535). Additionally, mutual inductance L_m is derived by the frequency characteristics when the transmitting distance is 150 mm. The coupling coefficient k of 0.09 is calculated from the inductance L and the mutual inductance L_m using $k = L_m/L$. The transmitting coil and the receiving coil have a same structure. In order to stabilize the figures of the windings, the windings are implemented to the grooves on the fixture which made from the acrylic. The resonance coils have a same structure to the helical antenna. Thus, the resonance coils have a feeding point at the center of the resonance coil such as a dipole antenna. It means that both of the coil-ends are open. In consequence, the resonance coils have a self-resonant frequency f_0 owing to the distributed capacitance C of the winding pitch and the winding inductance L. The self-resonance frequency is obtained by

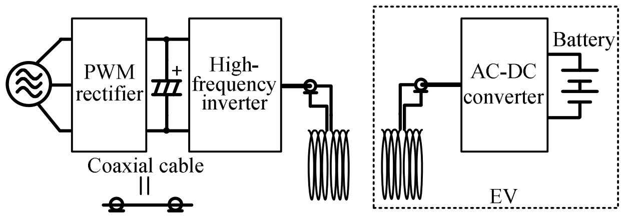

Fig. 1. The configuration example of the wireless power transfer system.

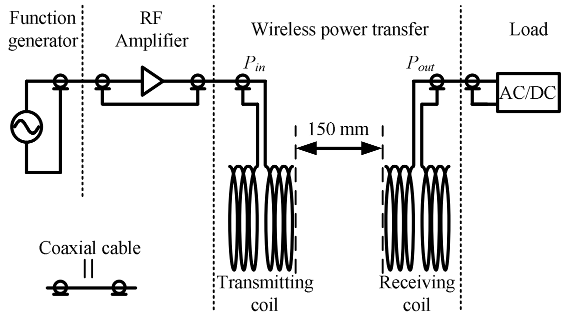

Fig. 2. System configuration of the experimental setup.

Table 1. The specifications of the resonance coils.

Number of turn	6 [turn]
Material	Magnet wire φ2.3[mm]
Radius	20 [cm]
Length	9.9 [cm]
Ohmic resistance R_{ohm}	151 [mΩ]
Inductance L	66.0 [μH]
Capacitance C	3.0 [pF]
Mutual inductance L_m	6.3 [μH]

$$f_0 = \frac{1}{2\pi\sqrt{LC}} \quad \text{.......} (2)$$

Fig. 3 presents the equivalent circuit of the wireless power transfer with MRC using open-end helical coils. The equivalent circuit of the one-sided open-end helical coil is obtained as a series RLC circuit because a winding capacitance in helical coils is represented as series capacitor[20]. Thus, MRC has a same equivalent circuit to the electromagnetic induction, which has series resonance capacitors in the both sides; transmitting and receiving sides. It should be noted that the equivalent circuits of the MRC are different between the short-end transmission coil and the open-end transmission coil. The equivalent circuit of the short-end transmission coil is obtained as a parallel resonance circuit. On the other hand, the equivalent circuit of the open-end transmission coil is presented as a series resonance circuit.

Equation (3) provides the transmitting efficiency, where $S_{21}(\omega)$ is the transmission coefficient obtained by (4)[20], R is the sum of the simulated resistance of a radiation loss, an ohmic loss of the resonance coils and a dielectric loss which occurs in the braces of the resonance coils, Z_0 is the load impedance and the output impedance of the power supply, and ω is the transmission angular frequency.

$$\eta(\omega) = \left|S_{21}(\omega)\right|^2 \times 100 \quad \text{.......} (3)$$

$$S_{21}(\omega) = 2jL_m Z_0 \omega \Bigg/ \left[L_m^2 \omega^2 - \left\{ R + \left(\omega L - \frac{1}{\omega C} \right) \right\}^2 + 2jZ_0 \left\{ R + \left(\omega L - \frac{1}{\omega C} \right) \right\} + Z_0^2 \right] \quad \text{.......} (4)$$

The transmission coefficient is proportional to the transmitted power to the travelling power. By substituting the resonance angular frequency ω_m and ω_e into (4), (5) is obtained[21] when the term of simulated resistance R is assumed zero.

$$S_{21}(\omega_m) = \frac{2}{2 - j\dfrac{1}{kQ}}, \; S_{21}(\omega_e) = \frac{2}{2 + j\dfrac{1}{kQ}} \quad \text{.......} (5)$$

When the transmission frequency is equal to the resonance frequency of ω_m and ω_e, the transmission coefficient has local maximum value. Beside, (5) indicates that the product of inductive coupling coefficient k between the primary and the secondary side and quality factor Q of the transmission coils affects the transmission efficiency. It should be noted that the (5) is valid only when an output impedance of the power supply is equal to the load impedance. Generally, the transmission efficiency using the electromagnetic induction method is not so high in a middle-range transmission distance because a coupling coefficient k decreases inversely with a cube of transmission distance. In contrast, the high quality factor Q allows high efficiency wireless power transfer in the MRC even when a coupling coefficient has a small value.

3. Conventional Rectifiers with Wide-band Gap Semiconductor Devices

Considering the application to EV chargers requires an AC-DC converter which converts power from high-frequency AC to DC in the receiving side. In this chapter, the experimental results with a conventional CI-DBR as AC-DC converters in the receiving side are shown. In addition, the power losses are separated to a transmission loss, a reflection loss and a conversion loss of the CI-DBR.

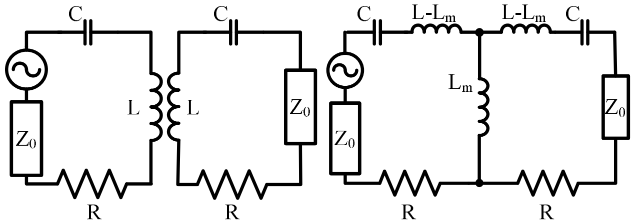

(a) Equivalent circuit. (b) Equivalent circuit of type-T.

Fig. 3. Equivalent circuits of the wireless power transfer with MRC.

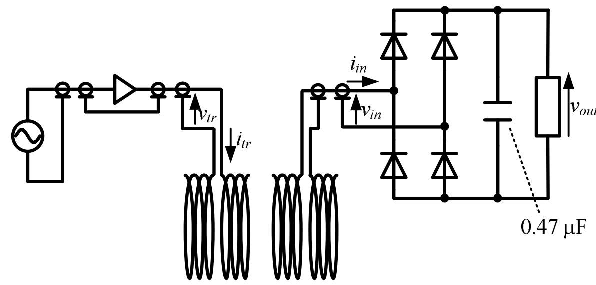

Fig. 4. Experimental setup with conventional diode bridge rectifier.

Table 2. Ratings of the diodes for CI-DBR shown in Fig. 4.

Diode	Rated voltage V_R [V]	Rated current I_F [A]	Forward voltage drop V_F [V]
SiC-SBD	600	4	1.8
GaN-diode		6	1.9
Si-FRD		3	3

3.1 Experimental Setup Fig. 4 presents the experimental setup with conventional CI-DBR where v_{tr} is the transmitting coil voltage, i_{tr} is the transmitting coil current, v_{in} is the receiving coil voltage, i_{in} is the receiving coil current and v_{out} is the rectifier output voltage. The SiC or GaN diodes are used as power devices in order to achieve a high-frequency operation of the rectifiers because the switching devices with wide-band gap semiconductors such as SiC and GaN are suitable for a high-frequency operation[22-25]. The ratings of the power devices which have voltage rating of 600 V and the current rating of several amperes are shown in Table 2. Note that the schottky barrier diode (SBD) is chosen for SiC. Additionally, the fast recovery diode (FRD) is used for Si device in order to compare the characteristics of the rectifiers. The forward voltage drops of the diodes at the rated currents and a junction temperature of 25 deg are described in the each datasheets.

The rectifiers are mounted on the each printed circuit boards (PCB) for a high frequency operation. The rectifiers have an input terminal of a coaxial connector. Accordingly, the rectifier is connected using a coaxial cable which has characteristics impedance of 50 Ω to operate in a high-frequency. In addition, the laminated ceramic capacitor of 0.47 μF (Murata, GRM43DR72E474KW01L) is used as a smoothing capacitor in purpose of smoothing the high-frequency voltage ripples.

3.2 Experimental Verifications with CI-DBR Fig. 5 presents the operation waveforms of the rectifiers, which uses the SiC, GaN and Si diodes when the transmission frequency is 11.18 MHz, the load resistance of the rectifiers is 100 Ω, the travelling power is 100 W and the transmission distance is 150 mm. Note that, the resonance frequency does not agree with a 13.56 MHz in these experiments because the resonance frequency depends on the transmission distance.

From Fig. 5 (a) (b), the rectifier input voltage v_{in} includes large harmonics components. Generally, when CI-DBRs are operated by ideal voltage source, it is known that CI-DBRs have an input current with large harmonics components. However, only fundamental component is efficiently delivered from the transmitting side to the receiving side in this experimental setup because the wireless power transfer systems with MRC have large quality factor Q. It means that any frequency components excepting the resonance frequency cannot be transmitted by wireless power transfer with MRC. Thus, the input voltage of rectifier has large distortion.

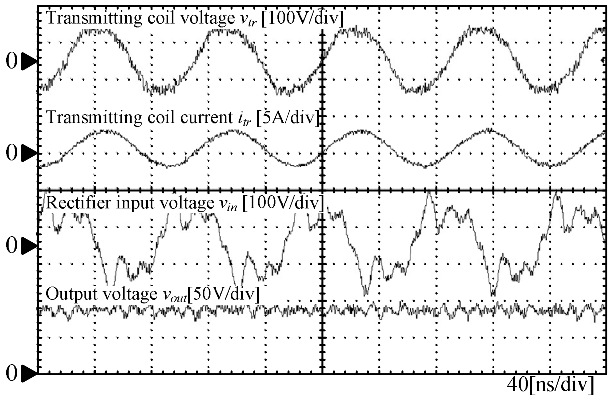

(a) With SiC-SBDs.

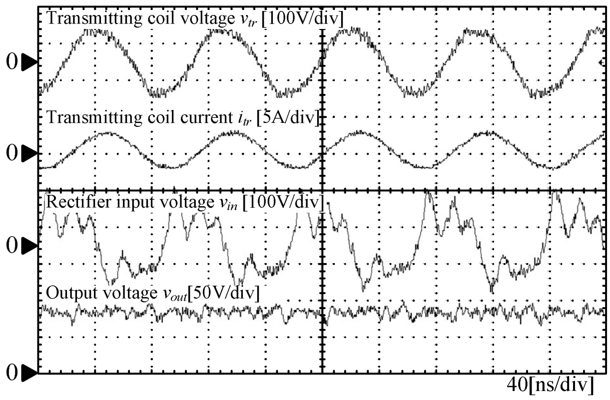

(b) With GaN-diodes.

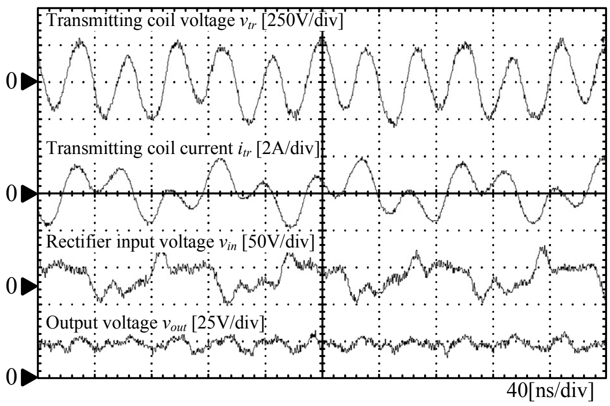

(c) With Si-FRDs.

Fig. 5. Experimental waveforms when the conventional CI-DBR is connected to the wireless power transfer using MRC as a load.

Focusing on the output voltage v_{out}, the DC voltages with low voltage ripples are obtained when the SiC and GaN diodes are used as shown in Fig. 5 (a) and (b). On the other hand, the DC voltage has large voltage ripples when the Si diode is used as shown in (c). The voltage ripples are 34.1% with SiC-SBDs, 38.5% with GaN-diodes and 78.6% with Si-FRDs respectively.

When the Si-FRD is used as a switching device, a limitation of the switching speed narrows the conduction time of the diodes. The shortening of the conduction time is verified by the increase of output voltage ripple. The shortening of the conduction time means the increase of input impedance of the CI-DBR. Thus, much reflected power occurs rather than the others CI-DBR.

The transmitting coil voltage includes a large component of second harmonics from the transmission frequency due to the standing wave. Generally, the standing wave which is synthetic wave of the travelling power and reflected power becomes the loss in transmission line. Furthermore, the standing wave causes a radiation of electromagnetic wave from transmission lines. So, the reflected power which causes a standing wave should be suppressed.

The total efficiency which includes the transmission loss, reflection loss and conversion loss, that is obtained from the wireless power transfer system with SiC, GaN and Si diodes, can reach to 75.2%, 69.2% and 5.2% respectively. The experimental results verified that the wide-band gap semiconductor devices are more suitable for the wireless power transfer system than Si device.

3.3 Power Loss Separation Fig. 6 shows a bar chart that indicates the loss of the wireless power transfer system including the diode rectifiers using the SiC and GaN diodes. Each loss is separated according to loss separation method shown in Ref. (19).

The SiC and GaN follow the similar characteristics. The conversion loss of the rectifier using the SiC or GaN decreases with an increase in load resistance. This can determine that a conduction loss of the diodes dominates a conversion loss. The difference of the forward voltage drops widely affects the conversion losses. In this experiment, the conversion efficiency with SiC-SBD is higher than the GaN-diodes.

Moreover, the conduction loss of the diodes decreases with the increase in load resistance because the input travelling power has configured constantly. Beside the sum of the reflection loss of the resonance coils dominates an over half of the total loss. It should be noted that the sum of the reflection loss become minimum at the load resistance of 50 Ω. The reflection loss of the transmitting coils can be reduced because the reflection loss depends on the impedance of the resonance coils, which depends on the shape and materials of the resonance coils.

On the other hand, the reflected power depends on the input impedance of a CI-DBR. The input impedance of the CI-DBR fails to match to the characteristic impedance due to the input current with large distortion. Moreover, the input current has fluctuation due to the load of the CI-DBR. In order to increase the efficiency, the input impedance should be matched to the characteristic impedance of the transmission line regardless of load conditions. In the next chapter, the conditions of the impedance matching are described.

4. AC-DC Converter with Input Impedance Matching

4.1 Required Input Impedance Matching Generally, high-frequency circuits are constructed with an impedance matching. Namely, a characteristic impedance of the power supply and the input impedance have same impedances to the characteristic impedance of the transmission line. In particular, the characteristic impedance of 50 Ω is used widely. Thus the 50 Ω is used in this paper. Besides, the input impedance of AC-DC converters with a battery is required to implement an impedance matching regardless of load conditions.

Generally, a characteristic impedance of transmission lines which is a reference value for the input impedance of the AC-DC converter, do not include an imaginary part. It means that the 50 Ω of the characteristic impedance implies the $50 + j0$ Ω. Therefore, input voltage and current of the AC-DC converter are required to fulfill the following conditions.

(a) $V_{in}/I_{in} = 50$ Ω

(b) Input power factor is 1 ($\cos\theta = 1$)

where V_{in} is the fundamental input voltage of the AC-DC converter, I_{in} is the fundamental input current and θ is the phase angle between the input voltage and the input current. In a low-frequency region, power factor correction (PFC) circuits with a PWM control are used widely[26-30]. The PFC circuits can satisfy the above-mentioned conditions due to the input current control with the PWM. However, the PWM needs high-frequency switching compared with an input frequency. Thus, it is difficult to operate the conventional PFC circuits when the input frequency is constrained to high-frequency such as 13.56 MHz in the wireless power transfer system. As a result, an AC-DC converter without a high-frequency switching is required in the receiving side of the wireless power transfer system.

4.2 Circuit Configuration Fig. 7 shows the circuit configuration of the proposed AC-DC converter. The proposed converter consists of a resonant-type rectifier which is reported by K. Matsui et al.[31-32] and a bidirectional boost chopper. The resonant-type rectifier achieves the PFC operation using the resonance between the inductor which is connected in series to the input terminal and the capacitors in parallel to the upper arm. The resonant-type rectifier has been demonstrated in a commercial frequency in Ref. (31). However, this converter becomes a low power density in the low-frequency operation because a huge inductor and capacitors as resonance components are required. Additionally, the possibility of the input impedance matching is not discussed. In this paper, the resonant-type rectifier is operated at a high-frequency and the function of the input impedance matching is evaluated. The high-frequency operation improves the power density owing to the downsizing of the passive components.

In addition, Ref. (32) pointed that the amplitude of the input current and the input power factor are changed by load conditions when a resistance load is connected directly to the resonant-type rectifier. It means that the input impedance of the stand-alone resonant-type rectifier depends on the load conditions widely. In

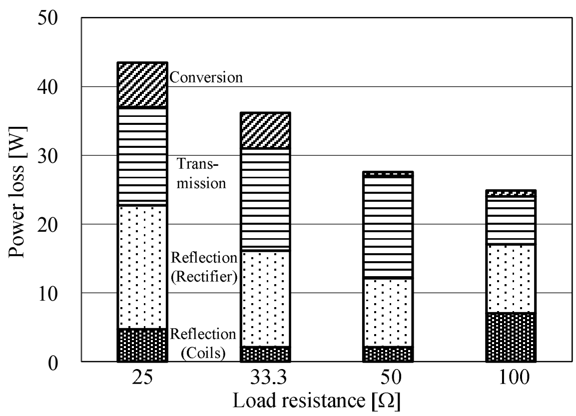

(a) With SiC-SBD.

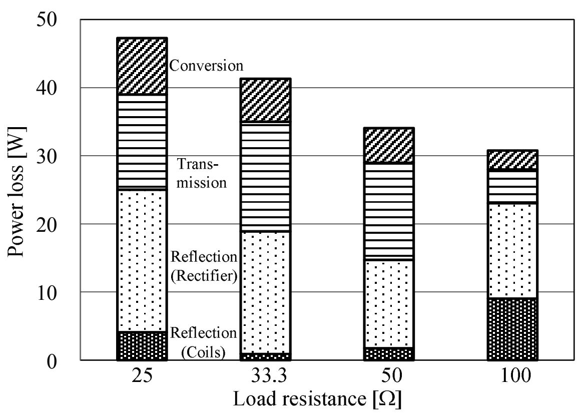

(b) With GaN-diodes.

Fig. 6. Loss separation results of the wireless power transmission system with CI-DBR.

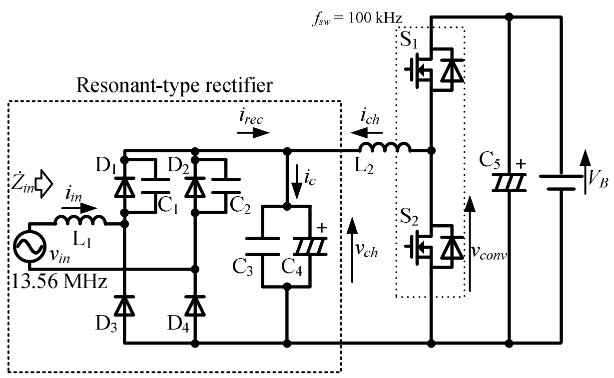

Fig. 7. The proposed AC-DC converter with input impedance matching for a high-frequency wireless power transfer system.

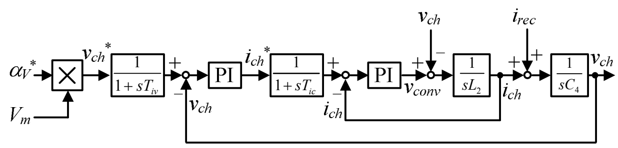

Fig. 8. Control block diagram for S_1 and S_2 in the proposed AC-DC converter.

order to overcome this problem, the bidirectional boost chopper is connected at the rear side of the resonant-type rectifier in Fig. 1. The bidirectional boost chopper is operated in purpose to fix the operating point which is decided by the rectifier output voltage v_{ch} of the resonant-type rectifier. The MOSFET S_1 is used for an initial charge of the C_4 instead of a diode because the input power factor closes to zero when the rectifier output voltage v_{ch} is around zero.

The input impedance is determined by the input voltage and input current. Therefore, the bidirectional boost chopper controls the ratio between the input voltage and input current in the proposed circuit. On the other hand, the phase angle is fixed at a resonance point in the rectifier in order to achieve the imaginary part of zero. In detail, the input impedance of the proposed circuit is determined by the three parameters; the resonance inductance L_1, the resonance capacitance C_1, C_2 and a voltage ratio α_V where the voltage ratio is the ratio of the rectifier output voltage v_{ch} to the input maximum voltage V_m. The voltage ratio should be constant in order to achieve the intended input impedance. Note that, the voltage ratio, which achieves the intended input impedance, depends on the combination of the resonance capacitance and resonance inductance. The control method of the rectifier output voltage is shown in the next subsection.

The control for the chopper circuit does not need a high dynamic response. Thus, the chopper circuit does not need neither high-speed nor high-frequency switching. Thus, the chopper may be operated in a low switching frequency such as 20 kHz. However, a switching frequency of 100 kHz is selected in this paper with the objective of the downsizing of the inductor L_2 in Fig. 1. Note that, the SiC schottky barrier diodes (SiC-SBDs) are used in the rectifier because rectifying diodes are required to have a performance to rectify the 13.56-MHz AC.

4.3 Control Method of Bidirectional Boost Chopper

Fig. 8 shows a control block diagram of the bidirectional boost chopper where T_{ic} is the integral action time of an automatic current regulator (ACR) and T_{iv} is the integral action time of an automatic voltage regulator (AVR). The bidirectional boost chopper is operated in order to stabilize the voltage ratio α_V. Thus, the reference value of the rectifier output voltage is provided as

$v_{ch}^* = V_m \times \alpha_V^*$.

Note that, the capacitance C_3 can be negligible because the capacitance C_3 dominant in the combined capacitance of the capacitors C_3 and C_4. The resonant-type rectifier achieves a PFC operation regardless of the battery voltage V_B. This is attributed to an ACR in chopper current i_c and an AVR in the rectifier output voltage v_{ch} of the bidirectional boost chopper. Namely it is assumed that the voltage source is connected to the rear end of the resonant-type rectifier.

In the proposed circuit, a fast dynamic response of the bidirectional boost chopper is not necessary. So, the AVR control is constructed by a PI control with a natural angular frequency of 400 rad/s. Also the ACR is constructed by a PI control with 4000 rad/s as an inner loop in the AVR. The input current from the rectifier i_{rec} is deal as a disturbance. The input impedance of the proposed AC-DC converter is determined by the resonant capacitors and the inductor. The design method of these parameters is omitted in this paper because of space limitations.

5. Simulation Results of the Proposed AC-DC Converter

Fig. 9 presents the simulation results of the AC-DC converter where the input voltage is 223 V, rated input power is 1 kVA. The chopper current i_{ch} and the chopper voltage v_{ch} track the referenced chopper current i_{ch}^* and the referenced rectifier output voltage v_{ch}^* respectively. It looks like the chopper current does not track to the reference value. On the contrary, the input current tracks to its reference value completely. It is caused by the low switching frequency of the chopper circuit.

The rectifier output voltage includes second harmonic components from the input frequency because the capacitor C_3 is charged by the rectifier current i_{rec}. The difference of the impedance between the capacitor C_3 and L_2 allows the rectifier current to flow into only the capacitor C_3.

Focusing on the Fig. 9, the input current with a sinusoidal waveform of the AC-DC converter is obtained because the voltage control over the rectifier output. Additionally, the input power factor of the AC-DC converter is closed to 1 approximately. Thus, an absolute value of the input impedance $|\dot{Z}_{in}|$ is calculated as 49.6 Ω from the simulation results; the fundamental input voltage is 223.4 V, and the fundamental input current is 4.50 A. The input impedance is focused based on the fundamental component because the wireless power transfer with high quality factor Q enable a power transmission without harmonics components. The input impedance is calculated from the fundamental component of the input voltage and input current as a 49.6 + j0 Ω. It means that the proposed converter is capable of the input impedance matching to the 50 + j0 Ω at the reflection coefficient which is defined by (6) of 0.4%.

$$\Gamma = \left| \frac{\dot{Z}_0 - \dot{Z}_{in}}{\dot{Z}_0 + \dot{Z}_{in}} \right| = \sqrt{\frac{P_R}{P_F}} \quad \text{(6)}$$

where $\dot{Z}_0$ is the characteristic impedance which is 50 + j0 Ω in this paper, P_F is the travelling power, P_R is the reflected power which are measured in the high-frequency power meter in the RF amplifier. The squared reflection coefficient means the ratio of reflected power to travelling power.

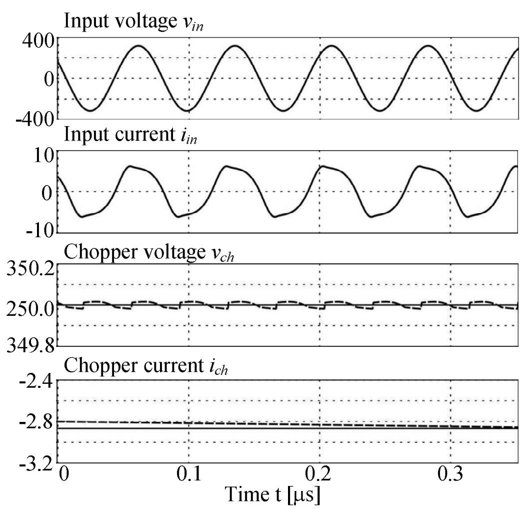

Fig. 9. Operation waveforms of the proposed AC-DC converter in simulation.

6. Experimental Results of the Proposed AC-DC Converter

6.1 Experimental Setup Experimental verifications are shown in this chapter. Table 3 provides the circuit parameters for the experimental setup. The circuit parameters, which affect the input impedance, are designed by cut and try because a relationship between the input impedance and these parameters is not linear. The design method of the resonance parameters will be shown in other paper.

The resonant capacitors are modified from 140 pF to 150 pF by reason of a convenience of procurement. Moreover, the inductor L_2 is made by authors from an electrical steel sheet core. Note that the bidirectional boost chopper in the proposed AC-DC converter is operated in open-loop control for simplicity. Also, a RF amplifier which has 50 Ω of output impedance is used instead of the receiving coil of the wireless power transfer system. Furthermore, the battery is simulated by the stabilized DC power supply, which cannot operate in a regeneration mode, with diode and a resistance for blocking a return of the current to the DC power supply.

The AC-DC converter; especially the part of the resonant-type rectifier is mounted on the printed circuit board (PCB) in order to cut down the effects of parasitic inductance and parasitic resistance between the circuit components. In particular, the parasitic inductance of a wire which is used in series to resonant inductance affects the input impedance. For this reason, the resonant-type rectifier should be mounted with keeping in mind of the parasitic inductances.

Besides, a laminated ceramic capacitor, which has low parasitic inductance in the high-frequency, is connected in parallel to the electrolytic capacitor in order to improve a characteristic of the smoothing capacitor C_4 because the rectifier voltage includes the second harmonics of the input frequency of 27.12 MHz. Similarly, the SiC-SBDs are used for a high-frequency operation of the resonant-type rectifier.

6.2 Experimental Waveforms Fig. 10 presents the operational waveforms of the proposed AC-DC converter where the simulated battery voltage V_B is set to 90 V. The experimental waveforms show that the input current can achieve a sinusoidal waveform with small distortion. Additionally, the input current has similar characteristics to the result which is obtained by using the simulation. Besides, DC voltages of the rectifier output voltage v_{ch} and the output voltage V_B are obtained. It means that the AC-DC converter enable the conversion from 13.56 MHz of AC to DC without a high-frequency switching. Note that, the input voltage distortion results from noises which are mixed into an input stage of the high-frequency power supply which used as instead of output coils of wireless power transfer system.

Table 3. Parameters of the circuit components.

Items		Manufactures	Model number	Value
MOSFET	S_1, S_2	Vishay	IRFB11N50APBF	500 V, 11 A
Diode	D_1-D_4	Cree	C3D08060A	600 V, 8 A
Inductor	L_1	TDK	VLF10040T-1R5N8R9 (Remodeled)	950 nH
	L_2	-	-	2.3 mH
Capacitor	C_1 C_2	TDK	C3216C0G2J151JT	150 pF
	C_3	TDK	CKG57NX7R2J474M	470 nF (in parallel)
	C_4	nichicon	UPW2V221MRD	220 µF (in parallel)
	C_5	BHC Components	ALS30A221DB450	220 µF

6.3 Harmonics analysis Fig. 11 indicates the harmonics analysis results of the input voltage and input current of the proposed AC-DC converter in the experiments. The harmonic analysis is performed with an oscilloscope in order to inspect the experimental waveforms. The input impedance of the proposed circuit is derived from the harmonics analysis. The input impedance is expressed by (7).

$$\dot{Z}_{in} = \frac{|V_{in\_1st}|}{|I_{in\_1st}|}\cos\theta + j\frac{|V_{in\_1st}|}{|I_{in\_1st}|}\sin\theta \quad (7)$$

where V_{in_1st} is the fundamental component of the input voltage, I_{in_1st} is the fundamental component of the input current, θ is the phase difference between the input voltage and the current on the fundamental harmonic.

The analysis results shown in Fig. 11 are scaled on the basis of

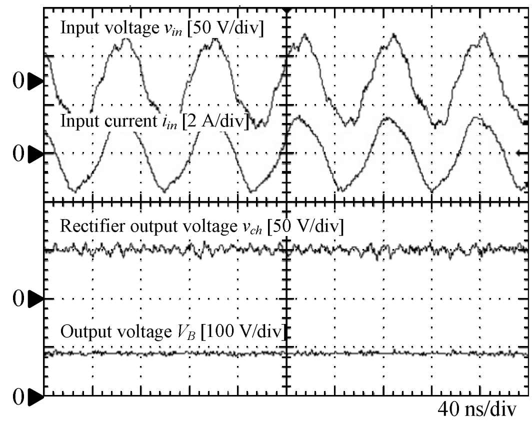

Fig. 10. Experimental waveforms of the proposed AC-DC converter.

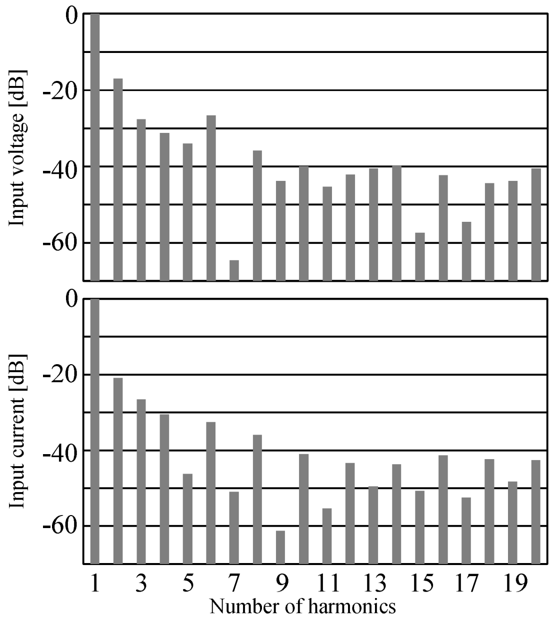

Fig. 11. Harmonics analysis of the input voltage and input current of the proposed AC-DCconverter.

amplitude at 13.56 MHz. Additionally, a sampling frequency of the oscilloscope is 1.25 GHz. Note that, the probes; a differential probe (Tektronix, P5205) and a current probe (Tektronix, TCP305), which are used in these experiments, provide a limitation to the frequency bandwidth at 100 MHz. For this reason, the harmonics components over 7th are considered as reference values. The input current harmonics is suppressed less than -20 dB in the frequency bandwidth from 2nd to 20th. Thus, the input current distortion (THD) is 11.2% (reference value) in the bandwidth by 20th from a 13.56 MHz.

Focusing into the fundamental components of the input voltage and current, the input voltage of 19.8 V and input current of 0.67 A are obtained from the harmonics analysis. It shows that an absolute value of the input impedance $|\dot{Z}_{in}|$ is 29.6 Ω. Also, 4.1 deg of phase difference between the input voltage and the input current is obtained. The phase angle presents the input power factor cos θ is 0.99. Hence, the input impedance of the proposed AC-DC converter is 29.6 + j0.51 Ω. The experimental results contain a measurable error in the real part since the design value is 50 + j0 Ω. An additional simulation results confirmed that the error occurs subject to the parasitic capacitances of the diodes of the resonant-type rectifier. A parameters design taking account of the parasitic capacitors can reduce the error and the reflection coefficient.

6.4 Comparison of the Reflection Coefficient Fig. 12 presents a comparison in terms of the reflection coefficient between the conventional CI-DBR with SiC-SBD shown in Fig. 4 and the proposed AC-DC converter.

It should be noted that all of reflection coefficient is measured in 13.56 MHz when the AC-DC converters are connected to the RF amplifier directly. The reflection coefficient should be zero because the reflected power is not input into a circuit.

The reflection coefficient of the CI-DBRs is measured at each of four different loads: 25 Ω, 33.3 Ω, 50 Ω and 100 Ω, because the input impedance of a conventional CI-DBR depends on the load condition. The proposed AC-DC converter minimizes the reflection coefficient among the others configuration with the conventional CI-DBR. Especially noteworthy is the fact that the reflection coefficient is suppressed by 37.8% in comparison with the CI-DBR with a load of 25 Ω. The experimental results show that the AC-DC converter can suppress the reflection loss which occurs at input side of the proposed AC-DC converter in

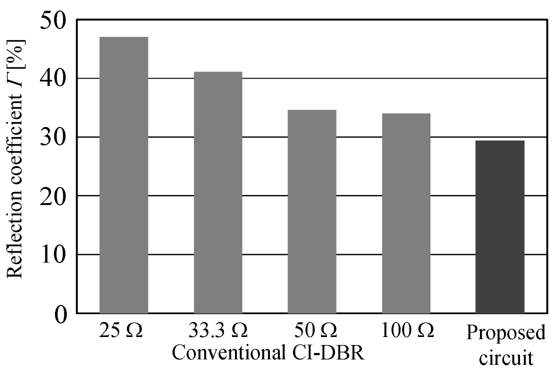

Fig. 12. Comparison of the reflection coefficients of the conventional CI-DBR and the proposed AC-DC converter based on the experimental results.

high-frequency wireless power transfer system. Furthermore, a design considering the parasitic capacitances of diodes in the resonant-type rectifier can further reduce the reflection coefficient.

7. Conclusion

In this paper, a reduction method of the reflected power is experimentally demonstrated using the AC-DC converters for a high-frequency wireless power transfer system with magnetic resonant coupling. A high-frequency AC-DC converter is required in the receiving side of the wireless power transfer systems which is operated at high-frequency such as 13.56 MHz. Additionally, the input impedance of an AC-DC converter should be matched to the characteristic impedance of the transmission line in order to reduce the reflection loss.

In order to apply the wireless power transfer into practical use, the CI-DBRs with SiC-SBDs and GaN diodes are tested. However, the loss separation results clarify that the reflection loss which occur at the input stage of the CI-DBRs drastically reduces the transmission efficiency because of the large harmonics and the load dependence of the input current. In order to solve the problem, the AC-DC converter, which that implements input impedance matching, is proposed. The experimental verifications confirmed that the proposed AC-DC converter enables a conversion from 13.56 MHz AC to DC without a high-frequency switching. In addition, the input impedance of 29.6 + j0.51 Ω is obtained from experiments. The reflection coefficient is reduced by 37.8% compared with the conventional CI-DBR with a load of 25 Ω. Thus, this is clear that the AC-DC converter is a valid circuit configuration to perform as a receiving side of the high-frequency wireless power transfer system.

In the future work, the detail of the design method of the proposed AC-DC converter will be optimized.

References

(1) U. K. Madawala, D. J. Thrimawithana: “A Bidirectional Inductive Power Interface for Electric Vehicles in V2G Systems”, *IEEE Trans. On Industrial Electronics*, Vol. 58, No. 10, pp. 4789-4796 (2011)

(2) J. J. Casanova, Z. N. Low, J. Lin: “A Loosely Coupled Planar Wireless Power System for Multiple Receivers”, *IEEE Trans. On Industrial Electronics*, Vol. 56, No. 8, pp. 3060-3068 (2009)

(3) S. A. Adnan, M. Amin, F. Kamran: “Wireless Power Transfer using Microwaves at 2.45 GHz ISM Band”, in *Proc. International Bhurban Conf. on Applied Sciences & Technology 2009*, pp. 99-102 (2009)

(4) F. Herbert: “Powersphere: A Photovoltaic Cavity Converter for Wireless Power Transmission using High Power Lasers”, in *Proc. 4th World Conference on Photovoltaic Energy Conversion 2006*, Vol. 1, pp. 126-129 (2006)

(5) K. Takayama: “CW 100 MW microwave power transfer in space”, in *Proc. Particle Accelerator Conf. 1991*, Vol. 4, pp. 2625-2627 (1991)

(6) F. Steinsiek, K. H. Weber, W. P. Foth, H. J. Foth, C. Schafer: “Wireless power transmission technology development and demonstrations”, in *Proc. 2nd International Conference on Recent Advances in Space Technologies*, pp. 140-149 (2005)

(7) A. Kurs, A. Karalis, R. Moffatt, J. D. Joannopoulos, P. Fisher, M. Soljacic: “Wireless Power Transfer via Strongly Coupled Magnetic Resonances”, *Science*, Vol. 317, pp. 83-86 (2007)

(8) A. Karalis, J. D. Joannopoulos, M. Soljacic: “Efficient Wireless non-radiative mid-range energy transfer”, *Annals of Physics*, Vol. 323, No. 1, pp. 34-48 (2008)

(9) S. Cheon, Y. Kim, S. Kang, M. L. Lee, J. Lee, T. Zyung: “Circuit-Model-Based Analysis of a Wireless Energy-Transfer System via Coupled Magnetic Resonances”, *IEEE Trans. On Industrial Electronics*, Vol. 58, No. 7, pp. 2906-2914 (2011)

(10) B. L. Cannon, J. F. Hoburg, D. D. Stancil, S. C. Goldstein: "Magnetic Resonant Coupling As a Potential Means for Wireless Power Transfer to Multiple Small Receivers", *IEEE Trans. On Power Electronics*, Vol. 24, No. 7, pp. 1819-1825 (2009)
(11) Z. N. Low, R. A. Chinga, R. Tseng, J. Lin: "Design and Test of a High-Power High-Efficiency Loosely Coupled Planar Wireless Power Transfer System", *IEEE Trans. On Industrial Electronics*, Vol. 56, No. 5, pp. 1802-1812 (2009)
(12) A. P. Sample, D. A. Meyer, J. R. Smith: "Analysis, Experimental results, and Range Adaptation of Magnetically Coupled Resonators for Wireless Power Transfer", *IEEE Trans. On Industrial Electronics*, Vol. 58, No. 2, pp. 544-554 (2011)
(13) C. K. Lee, W. X. Zhong, S. Y. R. Hui: "Effects of Magnetic Coupling of Nonadjacent Resonators on Wireless Power Domino-Resonator Systems", *IEEE Trans. On Power Electronics*, Vol. 27, No. 4, pp. 1905-1916 (2012)
(14) M. Kiani, U. Jow, M. Ghovanloo: "Design and Optimization of a 3-Coil Inductive Link for Efficient Wireless Power Transmission", *IEEE Trans. On Biomedical Circuits and Systems*, Vol. 5, No. 6, pp. 579-591 (2011)
(15) S. Lee, R. D. Lorenz: "Development and Validation of Model for 95%-Efficiency 200-W Wireless Power Transfer Over a 30-cm Air-gap", *IEEE Trans. On Industry Applications*, Vol. 47, No. 6, pp. 2495-2504 (2011)
(16) T. Imura, Y. Hori: "Maximizing Air Gap and Efficiency of Magnetic Resonant Coupling for Wireless Power Transfer Using Equivalent Circuit and Neumann Formula", *IEEE Trans. On Industrial Electronics*, Vol. 58, No. 10, pp. 4746-4752 (2011)
(17) Y. Hori: "Future Vehicle Society based on Electric Motor, Capacitor and Wireless Power Supply", in *Proc. International Power & Enegy Conf. 2010*, pp. 2930-2934 (2010)
(18) J. R. Long: "Monolithic Transformers for Silicon RF IC Design", *IEEE Trans. On Solid-state Circuits*, Vol. 35, No. 9, pp. 1368-1382 (2000)
(19) K. Kusaka, J. Itoh: "Experimental Verification of Rectifiers with SiC/GaN for Wireless Power Transfer Using a Magnetic Resonance Coupling", in *Proc. IEEE 9th Power Electronics and Drive Systems*, pp. 1094-1099 (2011)
(20) T. Imura, H. Okabe, T. Uchida, Y. Hori: "Study on Open and Short End Helical Antennas with Capacitor in Series of Wireless Power Transfer using Magnetic Resonant Couplings", in *Proc. Annual Conf. of the IEEE Industrial Electronics Society 2009*, pp. 3848-3853 (2009)
(21) T. Imura, H. Okabe, T. Uchida, Y. Hori: "Study of Magnetic and Electric Coupling for Contactless Power Transfer Using Equivalent Circuits", *IEE of Japan On Industry Applications*, Vol. 130, No. 1, pp. 84-92 (2010) (in Japanese)
(22) B. J. Baliga, M. Bhatnagar: "Comparison of 6H-SiC, 3C-SiC, and Si for power devices", *IEEE Trans. On Electron Devices*, Vol. 40, No. 3, pp. 645-655 (1993)
(23) A. M. Abou-Alfotouh, A. V. Radun, H. Chang, C. Winterhalter: "A 1-MHz Hard-Switched Silicon Carbide DC-DC Converter", *IEEE Trans. On Power Electronics*, Vol. 21, No. 4, pp. 880- 889 (2006)
(24) M. Ishida, Y. Uemoto, T. Ueda, T. Tanaka, D. Ueda: "GaN Power Switching Devices", in *Proc. IEEE International Power & Energy Conference 2010*, pp. 1014-1017 (2010)
(25) J. Everts, J. Das, J. V. Keybus, J. Genoe, M. Germain, J. Driesen: "A High-Efficiency, High-Frequency Boost Converter using Enhancement Mode GaN DHFETs on Silicon", in *Proc. IEEE Energy Conversion Congress & Exposition*, Vol. 4, pp. 3296-3302 (2010)
(26) K. Raggl, T. Nussbaumer, G. Doerig, J. Biela, J. W. Kolar: "Comprehensive Design and Optimization of a High-Power-Density Single-Phase Boost PFC", *IEEE Trans. On Industrial Electronics*, Vol. 56, No. 7, pp. 2574-2587 (2009)
(27) T. Nussbaumer, K. Raggl, J. W. Kolar: "Design Guidelines for Interleaved Single-Phase Boost PFC Circuits", *IEEE Trans. On Industrial Electronics*, Vol. 56, No. 7, pp. 2559-2573 (2009)
(28) J. Sun: "Input Impedance Analysis of Single-Phase PFC Converters", *IEEE Trans. On Power Electronics*, Vol. 20, No. 2, pp. 308-314 (2005)
(29) B. Singh, B. N. Singh, A. Chandra, K. Al-Haddad, A. Pandey, D. P. Kothari: "A Review of Single-Phase Improved Power Quality AC-DC Converters", *IEEE Trans. On Industrial Electronics*, Vol. 50, No. 5, pp. 962-981 (2003)
(30) M. M. Javanovic, Y. Jang: "State-of-the-Art, Single-Phase, Active Power-Factor-Correction Techniques for High-Power Applications - An Overview", *IEEE Trans. On Industrial Electronics*, Vol. 52, No. 3, pp. 701-708 (2005)
(31) K. Matsui, I. Yamamoto, K. Ando, G. Erdong: "A Novel High DC Voltage Generator by LC Resonance in Supply Frequency", in *Proc. European Conference on Power Electronics 2007*, pp. 1-8 (2007)
(32) I. Yamamoto, G. Erdong, M. Hasegawa, F. Ueda, H. Mori: "A High-DC Voltage Generator Using Rectifier Circuits with LC Resonance", in *Proc. IEEE International Conf. on Industrial Technology*, pp. 15-17 (2006)

Keisuke Kusaka

(Student Member) received his B.S. and M.S. degrees in electrical, electronics and information engineering from Nagaoka University of Technology, Niigata, Japan in 2011 and 2013, respectively. Since 2013, he is currently working towards to a PhD degree in electrical and electronics engineering. His research interests include high-frequency converters and wireless power transfer systems.

Jun-ichi Itoh

(Member) received his M.S. and PhD degrees in electrical and electronic systems engineering from Nagaoka University of Technology, Niigata, Japan in 1996 and 2000, respectively. From 1996 to 2004, he was with Fuji Electric Corporate Research and Development Ltd., Tokyo, Japan. Since 2004, He has been with Nagaoka University of Technology as an associate professor. He received the IEEJ Academic Promotion Award (IEEJ Technical Development Award) in 2007 and the Isao Takahashi Power Electronics Award in 2010. His research interests include matrix converters, DC/DC converters, power factor correction techniques and motor drives. He is a member of the Institute of Electrical Engineers of Japan and the Society of Automotive Engineers of Japan.